Journal of Cleaner Production 178 (2018) 22–33

Contents lists available at ScienceDirect

Journal of Cleaner Production

journal homepage: www.elsevier.com/locate/jclepro

Estimation of fly ash reactivity for use in alkali-activated cements - A step towards sustainable building material and waste utilization

J. Shekhovtsova [a, *], I. Zhernovsky [b], M. Kovtun [a], N. Kozhukhova [b], I. Zhernovskaya [c], E. Kearsley [a]

[a] Department of Civil Engineering, Faculty of Engineering, Built Environment & IT, University of Pretoria, South Africa
[b] Department of Materials Science and Technology, Institute of Architecture and Construction, Belgorod State Technological University named after VG Shukhov, Russia
[c] Department of Higher Mathematics, Institute of Economics and Management, Belgorod State Technological University named after VG Shukhov, Russia

ARTICLE INFO

Article history:
Received 14 August 2017
Received in revised form
28 November 2017
Accepted 30 December 2017
Available online 2 January 2018

Keywords:
Fly ash
Characterization
Alkali activated cement
Compressive strength

ABSTRACT

This paper addresses the detailed characterization of coal fly ashes with respect to their utilization in alkali-activated cement systems, thus maximizing the use of fly ashes in the construction industry. A technique was developed to estimate the reactivity of low calcium fly ashes in alkali-activated systems. The technique is based on a K-value which combines three characteristics of a fly ash. Two characteristics – amorphous phase percentage and specific surface area determined through Blaine measurement – are observed quantities. The third characteristic – degree of polymerization of silica in the amorphous phase of fly ash – is a calculated parameter. To take into account the water demand of fly ashes, which will influence the amount of water needed to get a workable mix, the shape factor was used to adjust the Blaine specific surface area. The relationship between the proposed K-value and compressive strength of alkali-activated fly ash pastes is approximated by a linear function. The correlation coefficient of the relationship varied from 0.961 to 0.833 for 1 and 91 days compressive strength respectively. The proposed K-value can firstly be used to rank fly ashes for their suitability to produce high strength alkali-activated materials and secondly when calibrated for a specific activator and curing conditions, to predict the compressive strength of alkali-activated fly ash binders.

1. Introduction

Human society strives for cleaner production by finding opportunities for re-cycling of waste materials instead of landfilling. In many countries, including South Africa, energy production relies on coal. The biggest problem is utilization of waste material, fly ash, produced during the production process. Eskom (power utility) and Sasol (petrochemical) are the largest coal processing companies in South Africa. Annually they generate about 30 Mt and 10 Mt of ash respectively. With two new coal based power stations to be commissioned in the next few years, the amount of ash generated annually will be even higher. Although ash can potentially be used as a cement extender, a component of brick making, filler in plastic and rubber, for soil amelioration, etc. ash is considered to be a waste product and the level of ash recycling in South Africa is rather low (less than 10% of produced ash), compared to the amount of waste generated. Millions of tonnes of ash are being stored and disposed in ash dams and landfills annually creating a pollution risk. Disposal of ash also requires the use of land which can be potentially utilized for agricultural purposes. Thus, utilization of ash is a very important global problem. Recycling of wastes (fly ashes, slags, etc.) in production of alkali-activated aluminosilicate materials could not only expand the raw materials base of the construction industry without increasing the use of natural mineral resources, but also reduce the effect of greenhouse gases associated with Ordinary Portland Cement and concrete production (McLellan et al., 2011; Yang et al., 2013).

Different initial products were found to be suitable for geopolymer and alkali-activated materials production, including thermally activated clays (Duxson et al., 2007), industrial slags (Fernández-Jiménez et al., 1999; Nazari and Sanjayan, 2015; Zhang

* Corresponding author. Department of Civil Engineering, University of Pretoria, Pretoria, 0002, South Africa.
E-mail addresses: j.shekhovtsova@gmail.com (J. Shekhovtsova), max.kovtun@up.ac.za (M. Kovtun).

https://doi.org/10.1016/j.jclepro.2017.12.270
0959-6526/

et al., 2017), fly and bottom ashes (Fernández-Jiménez and Palomo, 2003; Provis et al., 2009; Topçu et al., 2014), waste kaolin sludge (Longhi et al., 2016) used as a solo raw material, and slag, red mud or metakaolin etc. in a blend with fly ash (Nie et al., 2016; Wang et al., 2011; Zhang et al., 2014; Zhao et al., 2007) or combination of three and more feedstock (Zhuang et al., 2016). Coal fly ash is the particular interest of this study as more than 90% of all ash in South Africa is fly ash. It has been shown in recent studies that South African fly ashes are suitable for alkali-activation (Kovtun et al., 2016; Shekhovtsova et al., 2016, 2015, 2014). However, large-scale application of fly ashes in the production of alkali-activated materials is being held back by several technical issues, including the variability of the ash quality between power stations and even within one plant. This variability relates to inconsistency of the physical properties, chemical and mineralogical composition of coal as well as to the differences in the combustion process applied at each power station. In contrast to the production of Portland cement-based materials, where the quality of raw materials are controlled, fly ash variability makes it difficult to implement a standardized control of the output characteristics of fly ash as a raw material for geopolymer production. To maximize the use of fly ash in alkali-activated cement systems, the acceptance of alkali-activated materials by the construction industry is needed at industrial scale. To do so, it is important to determine key parameters affecting fly ash reactivity and develop a technique which will allow confident prediction of fly ash performance in alkali-activated systems and geopolymers.

Alkali activation of low calcium fly ashes is a complex process with multiple parameters being involved simultaneously. The kinetics of alkali activation (geopolymerization) depends on the chemical, mineral and phase composition of fly ash, the fineness of the fly ash, the type and concentration of alkaline activator and the curing temperature (Fernández-Jimenez et al., 2006; Fernández-Jiménez et al., 2006a, 2006b; Shekhovtsova et al., 2014). Fernández-Jiménez and Palomo (2003) reported that percentage of unburned material, amount of reactive silica, particle size distribution, and content of vitreous phase in fly ash are the most important factors influencing geopolymerization, which supported by Soutsos et al. (2016) who noted as well the importance of average grain size of fly ash. The main reaction product of alkali-activated fly ash is X-ray amorphous aluminosilicate gel (Palomo et al., 1999). This gel has been found to be responsible for the cementitious properties of the final material (Criado et al., 2008); and its quantity affects the mechanical strength of the final product (Zhang et al., 2013). The amorphous phase of each fly ash is not identical and the degree of solubility of the amorphous phase of fly ash in alkaline activators should play a significant role governing the alkali activation process. The quantity of amorphous fly ash phase is usually determined by Rietveld refinement of XRD data. The question is, 'Is it possible to estimate the quality of the amorphous phase?'

According to experimental investigations (Dalby and King, 2006; Kolb and Hansen, 1965; Lentz, 1964), theoretical studies (Fraser, 1977; Hess, 1977; Masson, 1977, 1968), modeling using molecular dynamics and statistical methods (Falk and Thomas, 1974; Lacy, 1965; Machacek et al., 2006; Sen and Tangeman, 2008), the structure of silicate melts is formed by discrete silicon oxide anions (Gramenitsky et al., 2000; Polyakov et al., 2010). An averaged amount of Si–O–Si bridges can be used as an integral parameter characterizing the structural condition of a glass phase. This parameter characterizes the degree of polymerization of silica in the glass phase of fly ash. The degree of polymerization associated with the chemical composition was mentioned previously by Kuryaeva (2004) for aluminosilicate glasses and melts. The degree of polymerization can be characterized by the coefficient $f = Si/O$, which can be determined as the ratio between silicon and oxygen ions in the glass in grams. Kuryaeva used a slightly different approach in estimating the structural conditions of aluminosilicate glasses by calculating the degree of depolymerization of a silicon-aluminum-oxygen network represented by the parameter NBO/T. This parameter is defined as the gram ratio between the ions of non-bridging oxygen (NBO) atoms and the ions of network formers per mole of glass $NBO/T = (2O-4T)/T$, where T – is network forming cations. It is known that dissociation of SiO_2-materials occurs more actively in the regions with lower degrees of polymerization (Dove et al., 2008). Koshukhova et al. (2014) showed that there is a consistent negative correlation between the degree of SiO_2-polymerization in the glass phase of fly ash and the compressive strength of fly ash geopolymers.

Fernández-Jimenez et al. (2006; 2006a) estimated fly ash reactivity showing that chemical analyses with selective solutions, Rietveld X-ray powder diffraction (XRD) quantification and nuclear magnetic resonance (NMR) were highly effective in not only characterizing and quantifying the phases present in fly ash (Fernández-Jimenez et al., 2006) but also in determining the degree of reaction of fly ash in alkaline media (Fernández-Jiménez et al., 2006a).

A further step in evaluating fly ash suitability for manufacturing geopolymer was done by Zhang et al. (2016) who proposed the use of an indexing approach, taking into account specific surface area, inter-particle volume and total concentration of network modifiers and formers in glassy phases. The authors drew a general trend, which shows the increase of compressive strength with reactivity index increase, however the need for more studies to further refine the parameters of the proposed index was emphasized. It is clear that despite the fact that many research groups studied the chemical, mineral and structural characteristics of low calcium fly ashes and their amorphous phase (Bumrongjaroen et al., 2007; Fernández-Jiménez et al., 2006a; Ward and French, 2006; Williams and Van Riessen, 2010), estimation of the reactivity of fly ashes during alkali activation needs further development.

In this paper, the suitability of eight South African fly ashes for alkali activation/geopolymerization is investigated. Some fly ashes used in the study show good performance in cement systems and are being recognized as commercial products. Other fly ashes do not comply with the requirements of International standards for use in concrete and currently are being discarded and landfilled. The aim of this study is to characterize and evaluate the potential of different fly ashes for use as a main source of aluminosilicates in alkali activation/geopolymerization. Based on theoretical knowledge and experimental results, the reactivity index or K-value is developed using physical, chemical and crystallographic properties of the studied fly ashes. The effect of the specific surface area, the quantity and the quality (the degree of polymerization) of the amorphous phase of fly ash, which are combined in the K-value, on compressive strength of alkali-activated fly ash pastes is studied. The proposed technique can potentially be used in future for initial estimation of fly ash reactivity in alkali-activated systems and possible strength prediction of fly ash-based alkali-activated materials. The ability to predict properties of alkali-activated materials produced from fly ash opens an opportunity to make power production a cleaner process by utilizing significant amount of by-product/waste, fly ash, in construction industry.

2. Materials and methods

Representative samples of fly ashes from eight different sources were used in this study. The chemical composition of fly ashes was

determined by means of X-ray fluorescence analysis. Samples of fly ashes were roasted at 1000 °C to determine loss on ignition (LOI). Afterwards $Li_2B_4O_7$ was added to roasted sample and they were fused into a bead. Beads were analyzed on the ARL Perform'X Sequential XRF Spectrometer using Quantas software.

The mineralogical composition of fly ashes was studied by X-ray diffraction. The samples for XRD analysis were prepared using a back loading preparation method. Small samples prepared for phase determination tests were pre-ground in a mill. After addition of 10% internal standard of Si (Aldrich 99% pure) for determination of crystalline and amorphous phase content, micronizing was done in a McCrone mill. Samples were analyzed using a PANalytical X'Pert Pro powder diffractometer with X'Celerator detector, variable divergence and receiving slits with Fe filtered Co-Kα radiation. The data was collected in the angular range $5° \leq 2\theta \leq 90°$ with a step size of 0.008° 2θ and a 13 s scan step time. Amorphous phase content was calculated according to procedure described by Fernández-Jimenez et al. (2006). Qualitative XRD analysis was done using a PDF-2 database. DDM v.1.95e software was used in a Derivative Difference Minimization (DDM) - algorithm mode for carrying out full-profile quantitative XRD analysis (Solovyov, 2004). The main advantage in using the DDM-algorithm for full-profile XRD computational procedures is the fact that there is no need to refine background parameters of the X-ray diffraction pattern. This significantly simplifies the procedure because the XRD background pattern of fly ash has a complex structure and approximation is a source of additional errors (Williams and Van Riessen, 2010). The crystal structures used for full-profile XRD analysis were taken from the Inorganic Crystal Structure Database (ICSD). The following codes were used as structural models: α-quartz 174, mullite 66445, magnetite 26410, hematite 15840, lime 61550, periclase 52026 and silicon 29288. The parameters optimized during full-profile analysis were: zero-shift error, sample shift, phase scale and lattice parameters. A pseudo-Voigt function was used. For dominant phases, anisotropic peak broadening parameters were refined instead of formal UVW parameters (Caglioti et al., 1958). Additionally, anisotropic peak broadening caused by micro-stresses was refined for silicon. Isotropic thermal parameters were optimized for silicon, α-quartz and mullite. For mullite, the atom site occupancy parameter was refined for Si, Al3, O3 and O4 atoms.

Physical characterization of fly ashes consisted of determination of fineness through Blaine air permeability and particles size distribution (PSD) tests. Laser diffraction granulometry was used to determine the particle size distributions (Mastersizer 2000, Malvern Instruments). Relative densities of fly ashes were measured by gas pycnometer (AccuPyc II 1340 Pycnometer, Micrometrics).

Surface morphology of fly ashes was studied by Scanning Electron Microscopy (SEM) imaging in secondary electron image mode. The fly ash surfaces were coated with carbon and investigated using a Zeiss Ultra Plus scanning microscope (Carl Zeiss, Germany) at 1 kV.

Geopolymer specimens were synthesized by adding a NaOH solution to fly ash. Since the fly ashes contain different amounts of amorphous and crystalline phases and thus the quantity of reactive SiO_2 and Al_2O_3 in the fly ashes varies, it was decided to keep the $Na_2O/Al_2O_3^{Amorph}$ molar ratio at 0.9 for all fly ashes. Typically better strength properties of alkali-activated systems are reported for mixtures with Na_2O/Al_2O_3 ratio of about 1 (Silva et al., 2007; Steveson and Sagoe-Crentsil, 2005). The $Al_2O_3^{Amorph}$ is the amount of Al_2O_3 in the amorphous phase of fly ash, as calculated by subtracting the contribution of the crystalline phases from XRF data (Rickard et al., 2011). Note that Na_2O content of fly ashes was not taken into account. All alkali-activated fly ash pastes were designed to have similar workability. Flow tests as for hydraulic cement mortar was adopted for alkali-activated fly ash pastes (ASTM C 1437, 2001). The water-to-fly ash ratio was chosen for each fly ash such that the flow of the alkali-activated fly ash paste would be in the range of 170–180 mm. After mixing sodium hydroxide solution with fly ash, pastes were cast into 40 × 40 × 160 mm prism moulds, compacted on a vibration table and subjected to curing at elevated temperature of 60 °C for 24 h, demoulded and kept at 25 ± 1 °C and relative humidity of 55 ± 5% until testing age. Mechanical properties of prisms were determined according to (SANS 50196-1, 2006). Samples were tested at 1 day (immediately after elevated temperature curing), 7, 28 and 91 days. Compressive strength results are expressed as a mean of six samples tested.

3. Results and discussion

3.1. Fly ash characterization

The performance of fly ash in alkali-activated materials is strongly dependent on the physical properties of the fly ashes, in particular fineness and surface area, which varies significantly from source to source. Usually, the higher the amount of smaller particles in a fly ash (all other parameters being the same), the higher the specific surface area would be, resulting in more contact for the reaction with the alkaline medium, thus causing a higher reaction rate and increased strength of the final material.

Particle size distribution of all studied fly ashes is shown in Fig. 1. It can be seen that fly ash C contains the highest amount of particles smaller than 45 μm, followed by fly ashes D, E, B, F, A, G and H. Clearly, fly ash C is the finest amongst all fly ashes with 50% of particles being smaller than 5 μm. All studied fly ashes can be divided into three groups according to fineness: 'fine' is presented by fly ash C, 'medium' - fly ashes D, E, B and F, and 'coarse' - fly ashes A, G and H.

Table 1 presents measured and calculated physical properties of the eight fly ashes. The results confirm that fly ash C is finest fly ash having the highest specific surface area, followed by fly ash D, B, E, F, G, A and H (in descending order).

Although particles size and fineness of fly ash are very important for the assessment of fly ash reactivity, particles shape should also be considered, as it affects the amount of water required to produce workable mixtures. In order to evaluate the particle shape of fly ashes numerically, a parameter known as 'the shape factor' will be introduced here. Hopkins and Cabrera (1984) proposed the use of a shape factor to characterize fly ash in relation to the ability to increase workability. A shape factor of 1.00 represents a perfect spherical shape, while higher values of the factor indicate non-

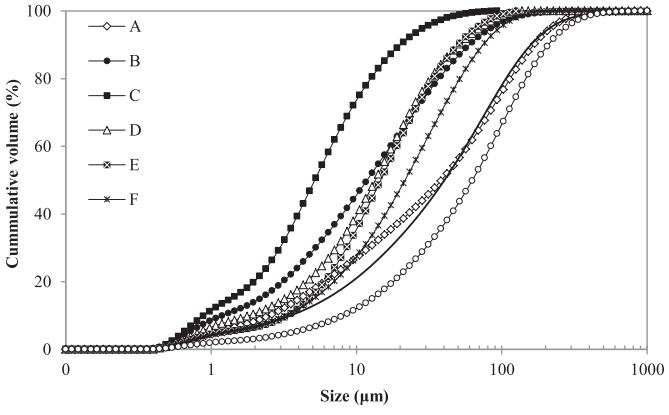

Fig. 1. Particle size distribution of fly ashes.

Table 1
Physical characteristics of fly ashes.

	A	B	C	D	E	F	G	H
Relative density	2.22	2.26	2.35	2.30	2.31	2.31	2.27	2.14
Blaine (m^2/kg)	232.2	316.2	452.4	368.0	303.6	292.7	247.1	171.6
Surface area calculated from PSD (m^2/kg)	183.6	304.5	445.8	303.4	192.9	178.1	158.9	79.3
Shape factor (ξ)	1.26	1.04	1.01	1.21	1.57	1.64	1.56	2.16
<45 μm, %	51.96	83.02	97.98	86.39	86.02	73.43	51.19	38.22
d_{10}, μm	2.6	1.3	0.8	1.9	3.2	3.2	3.5	8.6
d_{50}, μm	42	11	5	14	14	21	42	62
d_{90}, μm	168	62	21	51	51	76	168	226

spherical or angular particles. Agglomerated particles have shape factor smaller than 1. This parameter is a simple comparison of measured specific surface area, obtained in this study by using Blaine air permeability test, and the calculated specific surface area, derived from the particle size distribution by assuming that the ash consists of discrete spheres. The procedure for computation of surface area from the particle size distribution is described by Hunger and Brouwers (2009). Fig. 2 shows a graphical interpretation of the shape factor parameter. It can be seen that fly ashes C and B lies closely to the Blaine equals calculated surface area line, which means those fly ashes should have spherical shape particles. The greater the discrepancy between measured and calculated surface area, the greater amount of irregular or agglomerated particles in the fly ash. Shape factors (ξ) for all studied fly ashes are given in Table 1.

In order to evaluate fly ash surface morphology and validate the obtained shape factor, SEM image analysis was performed for all studied fly ashes. SEM micrographs of fly ashes are presented in Fig. 3. Fly ashes B and C have predominantly spherical shape and smooth surface, with fly ash C being much finer compared to all other ashes. Fly ashes A and D have notably less spherical particles, but also contain some agglomerates. Fly ashes E and F are quite fine and non-spherical in nature. Fly ashes G and H are the coarsest among all fly ashes with a high amount of large aggregates/agglomerates. At the same time fly ash H seems to have a rougher surface compared to fly ash G. The last four mentioned ashes (E, F, G and H) will have higher water requirements due to the shape, size and surface morphology of the particles compared to the first four fly ashes (A, B, C and D).

Chemical analysis results for the fly ashes are presented in Table 2. According to the chemical composition, all fly ashes are siliceous fly ashes as the amount of reactive calcium is less than 10%.

The geopolymerization process is highly dependent on the individual fly ash source (Duxson, 2009). Knowledge of the chemical and mineralogical composition of fly ashes is critical as not all

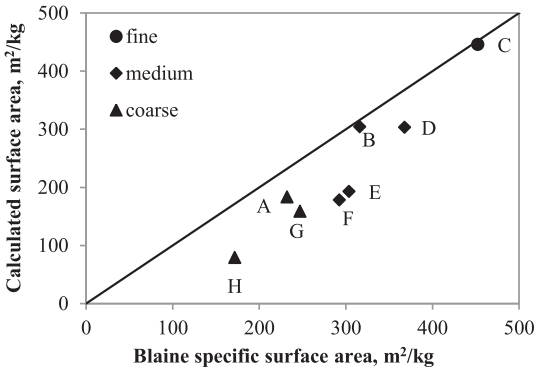

Fig. 2. Shape factor parameter chart.

alumina and silica takes part in the geopolymerization process (Van Jaarsveld et al., 1997). A detailed analysis of the mineralogical composition of each fly ash is presented in Table 3. An example of the full-profile XRD analysis performed for fly ash A is present in Fig. 4. Fly ashes consist mainly of amorphous phase with crystalline inclusions of mullite and quartz and minor amounts of other minerals (Table 3). The quantity of amorphous phase in fly ashes is of interest as it is the reactive part of any fly ash. Thus, fly ashes A, D and C have the highest content of amorphous phase, followed by H and B, which have moderate amorphous phase contents. Fly ashes F, G and E have the lowest amorphous phase contents at just more than 60% by weight.

The chemical composition of the amorphous phase of fly ashes was calculated by subtracting the contribution of the crystalline phases from XRF data using equations presented in Appendix A. The procedure used to determinate the chemical composition of the amorphous phase of fly ash was described by Ward and French (2006) as well as Rickard et al. (2011).

As mullite has variable chemical composition - $Al_{4+2x}Si_{2-2x}O_{10-x}$, the determination of SiO_2 and Al_2O_3 in mullite was performed for each fly ash using a refinement of Si and Al atom occupancy in positions of *Si*, *Al*3, *O*3 and *O*4 (66445-ICSD). Chemical formulas of mullite for each fly ash are presented in Table 4.

The estimated chemical compositions of the amorphous phase of fly ashes are presented in Table 5.

According to the chemical compositions of fly ash and amorphous phase presented in Tables 2 and 5 respectively, it can be seen that the SiO_2/Al_2O_3 ratio is higher and more variable for the amorphous phase of fly ashes compared to the fly ash itself. There is no clear correlation between $(SiO_2/Al_2O_3)^{Fly\ ash}$ and $(SiO_2/Al_2O_3)^{A\text{-}morph}$ (see Fig. 5).

The amorphous phase of fly ash is the most reactive part, playing an important role in the geopolymerization process. The structural characteristics of the amorphous phase will be different for all fly ashes due to fact that coal composition, combustion conditions and cooling process of ash vary. To characterize the structural condition of the amorphous phase of the fly ashes, the degree of polymerization of silica can be used. It is known that silica (SiO_2) is present in silicates and aluminosilicates in the form of silicon-oxygen tetrahedron $[SiO_4]^{4-}$ which form tetrahedral links. Thus, silicate tetrahedron properties can be linked to the degree of polymerization of the silicon-oxygen network. The coefficient f_{Si} is the measure of degree of polymerization and can be calculated using Equation (1) (Appen, 1974) with the estimated chemical composition of the amorphous phase (see Table 5).

$$f_{Si} = \frac{\gamma_{SiO_2}}{\gamma_{Me_2O} + \gamma_{MeO} + 3\gamma_{Me_2O_3} + 2\gamma_{MeO_2} + 5\gamma_{Me_2O_5} + 3\gamma_{MeO_3}} \quad (1)$$

where, γ - is the concentration of oxides in the amorphous phase of fly ash in mole fraction.

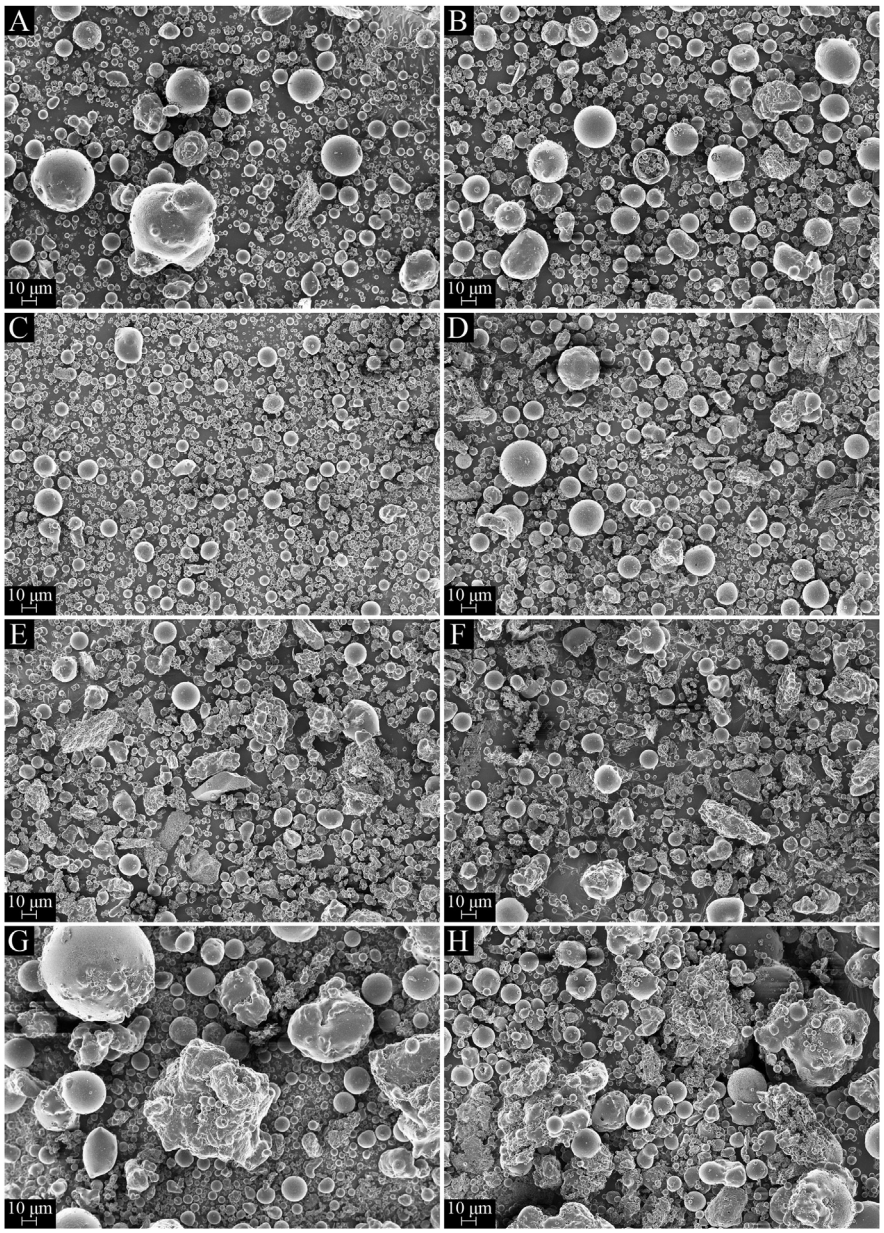

Fig. 3. SEM micrographs of fly ashes.

In the given equation, only Si^{4+} ions were taken into account to estimate the degree of polymerisation of amorphous phase, rather than Al^{3+} or other ions able to substitute silicon. The author of proposed equation gave well-reasoned example, where in $Na_2O\cdot Al_2O_3\cdot mSiO_2$ system at any *m*, the ratio between (Si + Al)/O is the same:

$$f_{Si+Al} = \frac{m+2}{2m+3+1} = 0.5 \quad (2)$$

Thus, any addition or removal of SiO_2 does not affect coefficient f_{Si+Al} or its inverse index - the oxygen number. The study of Dubrovo (1958) indirectly prove this statement, as no relationship between chemical resistance of glasses and the oxygen number could be obtained. At the same oxygen number huge difference in chemical resistance of glass in system $Na_2O–Al_2O_3–SiO_2$ was observed, and opposite at different oxygen numbers, the chemical resistance of glasses not infrequent was equal-order values. Thus, author concluded that calculation of f_{Si+Al} compared to f_{Si} do not affect properties forecast.

According to crystal chemistry of silicates, the value of the f_{Si} coefficient may vary from 0,25 to 0,5 (from $Q^0–[SiO_4]^{-4}$ to $Q^4–[SiO_2]^0$). The fewer siloxo-bonds in the amorphous phase of the fly ash (the lower value of f_{Si}), the more actively the fly ash will dissociate in an alkali medium (Dove et al., 2008). The coefficients f_{Si} for each fly ash calculated using Equation (1) is presented in Table 6.

According to these results fly ashes D and C have lower degrees of connectivity as f_{Si} for both fly ashes have the smallest values, followed by fly ashes F, G, A, B, E and H.

However, for estimating the fly ash reactivity it is necessary to take into account not only the degree of connectivity of the silicate tetrahedra in the amorphous phase of the fly ash, but also the concentration of the amorphous phase and the fly ash specific surface area, as a combination of these characteristics affects the fly

Table 2
Chemical composition of fly ashes.

	A	B	C	D	E	F	G	H
SiO_2	57.30	54.90	53.40	50.80	51.90	47.10	51.50	57.80
TiO_2	1.57	1.62	1.69	1.74	1.60	1.72	1.72	1.24
Al_2O_3	29.60	31.50	31.80	31.10	29.20	32.80	30.50	27.30
Fe_2O_3	3.89	3.53	3.69	3.50	3.05	3.22	4.70	6.13
MnO	0.04	0.04	0.03	0.04	0.06	0.04	0.05	0.08
MgO	0.89	1.00	1.12	1.49	1.41	1.90	1.49	0.68
CaO	4.79	4.55	4.59	5.78	7.55	7.67	6.49	3.45
Na_2O	0.20	0.40	0.26	0.11	0.31	<0.01	<0.01	<0.01
K_2O	0.86	0.83	0.92	1.06	1.19	0.59	0.91	0.98
P_2O_5	0.28	0.37	0.67	0.80	0.54	0.61	0.61	0.36
Cr_2O_3	0.03	0.04	0.06	0.04	0.03	0.02	0.03	0.02
V_2O_5	0.03	0.02	0.02	0.03	0.01	0.04	0.00	0.04
ZrO_2	0.04	0.04	0.03	0.05	0.04	0.05	0.05	0.05
SrO	0.12	0.13	0.15	0.32	0.27	0.22	0.20	0.08
WO_3	0.08	0.04	<0.01	<0.01	0.05	0.06	0.03	0.06
BaO	0.14	<0.01	0.16	0.22	0.16	0.14	0.14	<0.01
LOI	0.16	0.96	1.38	2.83	2.67	3.73	1.51	1.63

Table 3
Mineralogical composition of fly ashes.

	A	B	C	D	E	F	G	H
Quartz	10.0	9.4	8.5	7.2	10.6	5.5	9.9	9.0
Mullite	16.0	22.2	18.3	16.4	23.9	27.6	24.0	19.5
Magnetite	0.9	1.3	1.1	1.2	0.9	1.3	2.1	2.1
Hematite	–	–	–	1.0	1.2	0.8	1.2	1.6
Lime	–	0.5	0.5	0.6	1.0	0.7	0.4	–
Periclase	–	–	–	0.8	0.8	0.9	0.7	–
Amorphous	73.1	66.6	71.6	72.8	61.6	63.2	61.7	67.8

Table 4
Corrected composition of mullite.

	Chemical formula	$nAl_2O_3 \cdot mSiO_2$
A	$Al_4[Al_{0.618}Si_{1.382}O_{9.890}]$	2.309 Al_2O_3 · 1.382 SiO_2
B	$Al_4[Al_{0.592}Si_{1.406}O_{9.880}]$	2.296 Al_2O_3 · 1.406 SiO_2
C	$Al_4[Al_{0.603}Si_{1.397}O_{9.88}]$	2.302 Al_2O_3 · 1.397 SiO_2
D	$Al_4[Al_{0.586}Si_{1.413}O_{9.818}]$	2.293 Al_2O_3 · 1.413 SiO_2
E	$Al_4[Al_{0.556}Si_{1.443}O_{9.812}]$	2.278 Al_2O_3 · 1.443 SiO_2
F	$Al_4[Al_{0.520}Si_{1.479}O_{9.811}]$	2.260 Al_2O_3 · 1.479 SiO_2
G	$Al_4[Al_{0.430}Si_{1.470}O_{9.740}]$	2.215 Al_2O_3 · 1.470 SiO_2
H	$Al_4[Al_{0.526}Si_{1.474}O_{9.760}]$	2.263 Al_2O_3 · 1.474 SiO_2

Table 5
Chemical composition of fly ashes amorphous phase.

	A	B	C	D	E	F	G	H
SiO_2	58.90	60.02	56.82	55.85	58.75	56.73	57.35	65.03
TiO_2	2.14	2.45	2.40	2.48	2.70	2.88	2.83	1.86
Al_2O_3	24.27	23.01	25.97	27.15	19.91	21.54	21.80	19.80
Fe_2O_3	4.47	3.99	4.16	2.38	2.08	2.55	3.38	4.62
MnO	0.05	0.06	0.04	0.05	0.10	0.07	0.08	0.12
MgO	1.21	1.52	1.59	0.98	1.03	1.67	1.30	1.01
CaO	6.54	6.14	5.80	7.37	11.06	11.66	10.02	5.17
Na_2O	0.27	0.60	0.37	0.16	0.53	0.01	0.01	0.01
K_2O	1.17	1.25	1.31	1.51	2.01	0.99	1.49	1.47
P_2O_5	0.38	0.55	0.95	1.14	0.90	1.02	1.01	0.54
Cr_2O_3	0.04	0.06	0.09	0.05	0.05	0.03	0.05	0.03
V_2O_5	0.04	0.04	0.03	0.04	0.01	0.06	0.01	0.05
ZrO_2	0.05	0.05	0.04	0.06	0.07	0.08	0.08	0.08
SrO	0.17	0.20	0.21	0.45	0.45	0.36	0.32	0.12
WO_3	0.10	0.06	0.01	0.01	0.08	0.10	0.05	0.08
BaO	0.19	0.01	0.23	0.31	0.27	0.24	0.23	0.01

Note: The values have been normalized using amorphous phase content calculated as a sum of all oxides in the amorphous phase, but not the amorphous phase content presented in Table 3.

ash reactivity.

3.2. Compressive strength of alkali-activated fly ash pastes

The compressive strength of alkali-activated fly ash pastes at different ages is presented in Fig. 6. The error bars represent the deviation of the compressive strength from the mean of six samples tested.

The results show that all fly ashes developed some compressive strength after elevated temperature curing at 60 °C for 24 h. Fly ashes C, D, B and A produced pastes with relatively high strength of 60.3 MPa, 42.3 MPa, 35.9 MPa and 28.8 MPa respectively. While fly ashes E, F, G and H were responsible for much lower strength of 22.2 MPa, 18.4 MPa, 8.6 MPa and 3.6 MPa respectively.

Substantial strength increase over time was observed for all fly ashes. This confirms the findings of De Vargas et al. (2011) and Somna et al. (2011) that age has a significant effect on the strength of alkali-activated fly ash pastes, and the structural development does not stop with discontinuation of elevated temperature curing.

3.3. Effect of physical, mineralogical and structural condition of amorphous phase of fly ash on fly ash reactivity and behaviour in alkali-activated systems

The relationships between three characteristics of the fly ashes – specific surface area, amorphous phase content and the degree of polymerization – and the compressive strength of alkali-activated

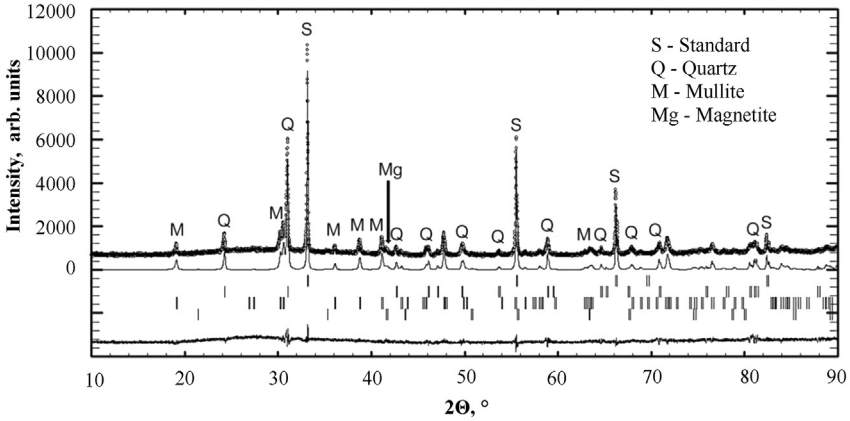

Fig. 4. Full-profile DDM-pattern of fly ash A.

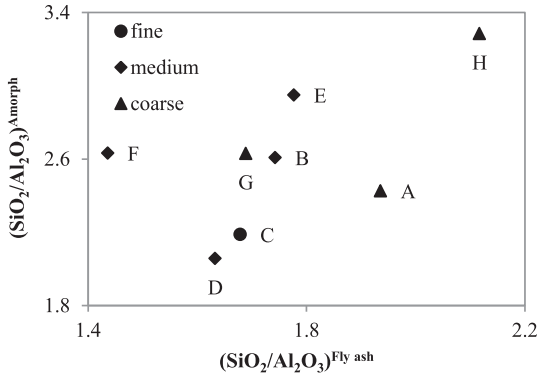

Fig. 5. Relationship of SiO_2/Al_2O_3 in the fly ashes vs. amorphous phase.

Table 6
Calculated degree of polymerization/connectivity of fly ash amorphous phase.

	A	B	C	D	E	F	G	H
f_{Si}	0.327	0.332	0.316	0.311	0.332	0.320	0.323	0.356

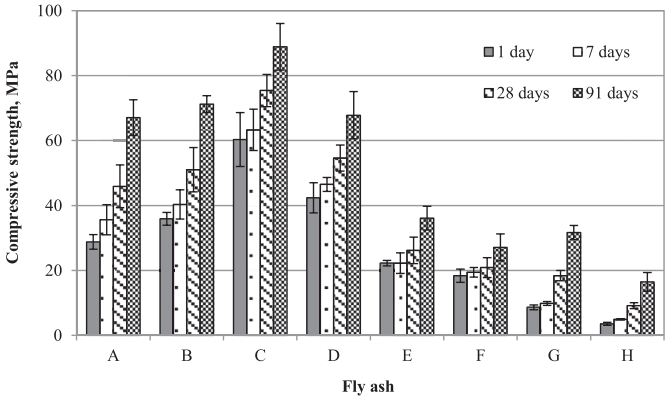

Fig. 6. Compressive strength of alkali-activated fly ash pastes.

fly ash pastes were analysed.

By analogy with cement, it is possible to assume that higher specific surface area of fly ash will produce alkali-activated fly ash paste with higher strength due to the greater contact area between aluminosilicate precursor and alkaline solution resulting in increased amounts of reaction products in the early age. The relationship between Blaine specific surface area of fly ashes and the compressive strength of alkali-activated fly ash pastes is given in Fig. 7.

Not all fly ashes are spherical in nature (see Fig. 3). Spherical particles are known to improve workability of mixtures, while angular or agglomerated particles require more water to produce workable mixture and as a result strength will be affected by the extra added water. The workability of all the alkali-activated fly ash pastes in this study were kept the same, which means the amount of water added to each fly ash was different. The shape factor of the fly ash should thus be considered to take into account the influence of fly ash particles morphology on the water demand of alkali-activated fly ash pastes. To do so, the Blaine specific surface area can be divided by the shape factor or, otherwise, the calculated surface area derived from the particle size distribution can be used. In Fig. 8 the correlation between the adjusted specific surface area and compressive strength of alkali-activated fly ash pastes at different age is presented.

It is necessary to note that linear regression of non-adjusted Blaine on the compressive strength of alkali-activated fly ash pastes produced significantly lower coefficients of determination (0.82; 0.75; 0.69 and 0.56 for 1 day, 7 day, 28 day and 91 day compressive strength respectively in Fig. 7) compared to those presented in the Fig. 8. Including the shape factor of fly ash significantly improved the level of prediction. There is a good correlation between adjusted specific surface area and 1-day compressive strength ($R^2 = 0.9348$). It can be seen that the effect of fineness of the fly ashes on the compressive strength of alkali-activated fly ash pastes is more pronounced at early ages (Figs. 7 and 8). This finding agrees with previously published results of Fernández-Jiménez and Palomo (2003) and Somna et al. (Somna et al., 2011) who concluded that fineness of fly ash plays an essential role in the strength development of alkali-activated fly ash, especially at the early age. It should be emphasized that the fact that the theoretical specific surface area has considerably better correlation with the strength development of alkali-activated fly ash cements, can make the evaluation process easier and more reliable because there would no need in the Blaine test which is much more dependent of an operator's skills than the PSD test.

It has been stated previously that the amount of vitreous phase in fly ash determines the fly ash reactivity for alkali activation (Fernández-Jiménez and Palomo, 2003; Winnefeld et al., 2010). Although no functional relationship between amorphous phase content and compressive strength was established (low R^2 value), there is positive correlation between these two values, which is increasing with the testing age (Fig. 9).

The effect of the f_{Si} coefficient on the compressive strength of alkali-activated fly ash pastes at different ages can be see in Fig. 10. The higher the value of the coefficient is, the less reactive fly ash.

Althoug there is no clear correlation between degree of polymerization (f_{Si}) and compressive strength of alkali-activated fly ash pastes in different age exponential regression was applied as a best fitted function.

It is desirable to incorporate the amorphous phase content with the surface area of fly ash, as surface area will determine physical availability/contact surface of amorphous phase for dissolution in alkaline solution. For characterization of fly ash reactivity and determination of suitability of the fly ash for alkali activation it is proposed to use a reactivity index, K-value, which can be determined using Equation (3):

$$K = \frac{S^{Measured}_{Specific}}{\xi} \cdot C_{Amorph} \cdot \exp(f_{Si}) \quad (3)$$

Or

$$K = S^{Theor}_{Specific} \cdot C_{Amorph} \cdot \exp(f_{Si})$$

where, $S^{Measured}_{Specific}$ – fly ash specific surface area, determined by Blaine air permeability method; $S^{Theor}_{Specific}$ – theoretical specific surface area, determined from particle size distribution analysis; ξ – the shape factor of fly ash, determined as a ratio between measured and calculated specific surface area; C_{Amorph} – concentration of fly ash amorphous phase; f_{Si} – degree of polymerization, determined according to Appen's formula (Equation (1)).

Fig. 11 shows the relationship between calculated K-value and the compressive strength of alkali-activated fly ash pastes at different age.

The proposed relationship has a high correlation coefficient and can be suggested for initial estimation of fly ash suitability for alkali activation. According to the obtained results, the K-value can be used for estimation of the performance of fly ash in alkali-activated

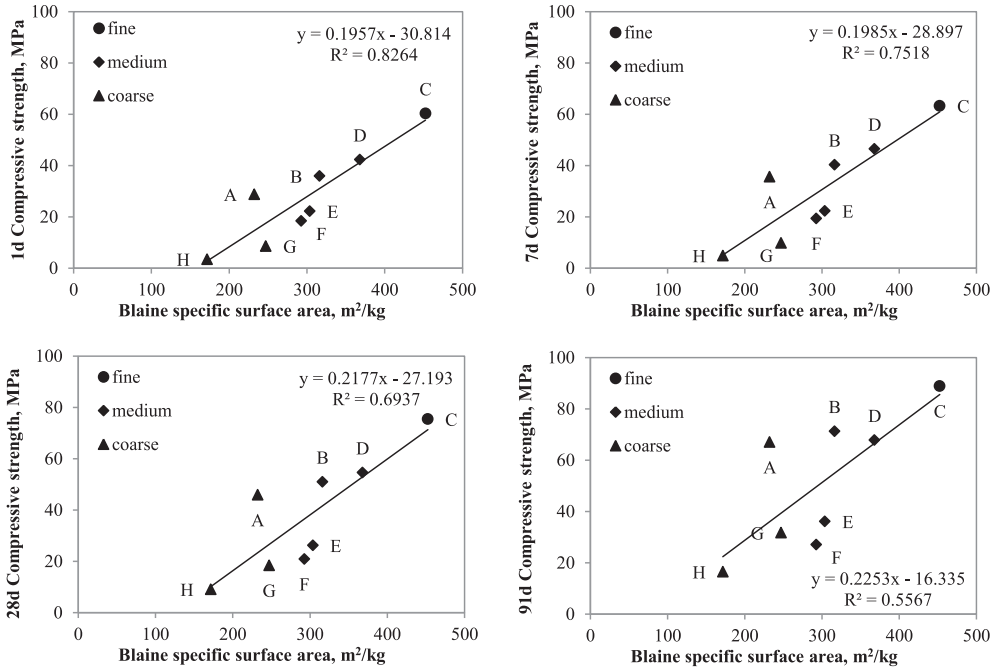

Fig. 7. Effect of Blaine specific surface area on strength of alkali-activated fly ash pastes.

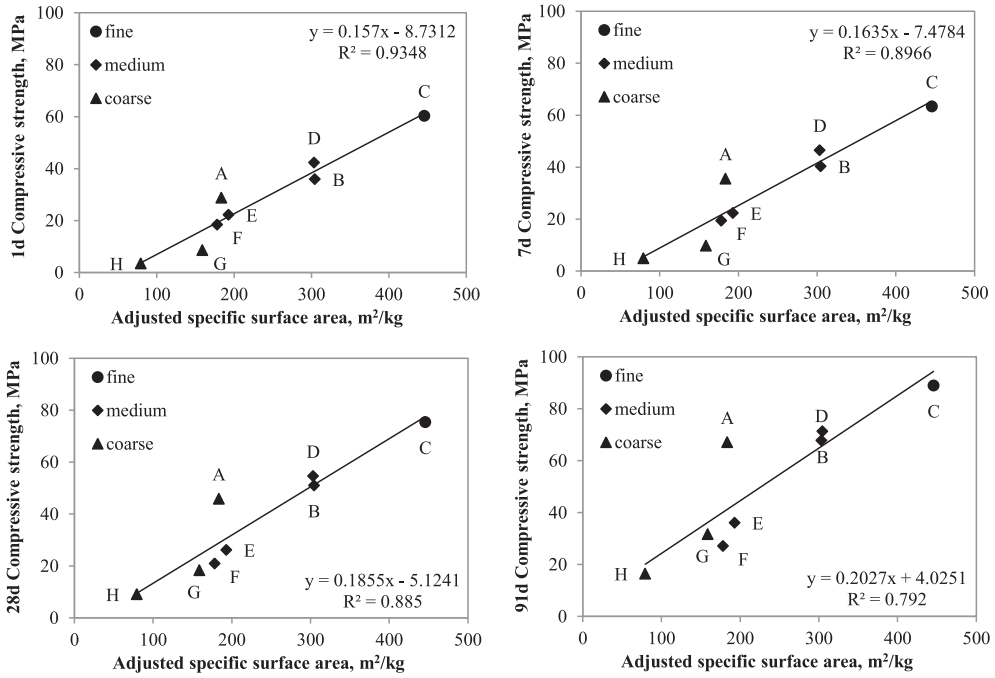

Fig. 8. Effect of adjusted specific surface area on strength of alkali-activated fly ash pastes.

systems with a high level of certainty at early ages. The coefficient of determination decrease with age, which might be explained by the fact that the influence of one or several factors (surface area, amorphous phase content and degree of polymerization of the amorphous phase) on the compressive strength decreases with age, possibly, due to ongoing structure formation in the alumosilicate gel (development of the pore structure, zeolite formation, etc.) which play a more dominant role with time. The contribution of each factor to the compressive strength development should still be investigated in future studies.

Further refinement of the K-value is needed to have better prediction of long-term strength development of alkali-activated fly ash cements. It is also important to validate the predictive technique against different sources of fly ash, type of activator and curing conditions used. Nevertheless, the results show that the K-value can be a powerful tool for evaluating and ranking fly ashes for production of alkali-activated materials.

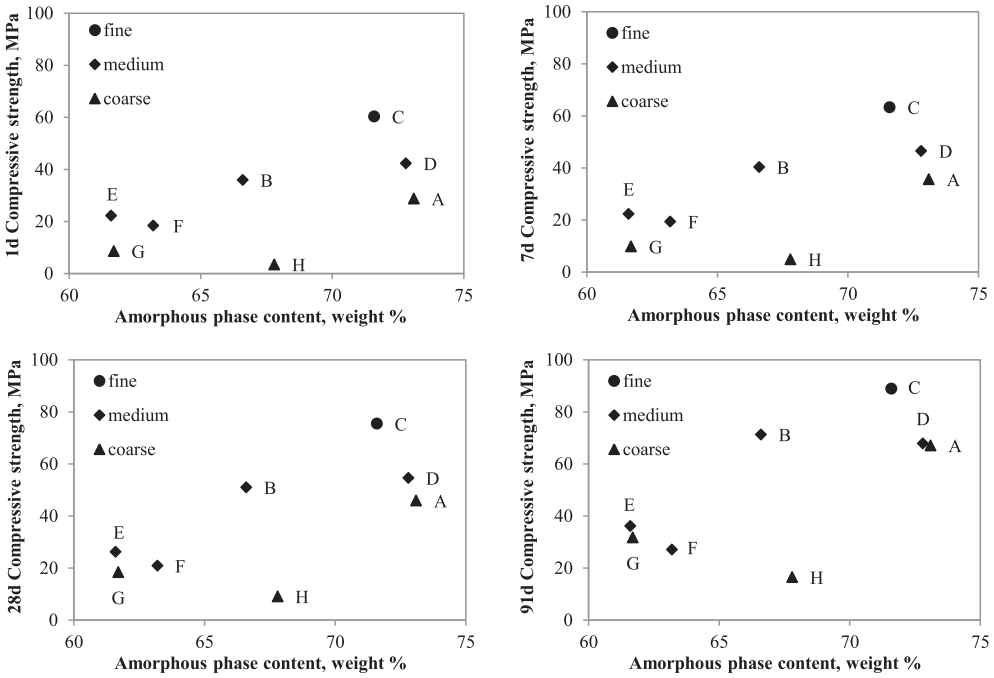

Fig. 9. Effect of fly ash amorphous phase on compressive strength of alkali-activated fly ash pastes.

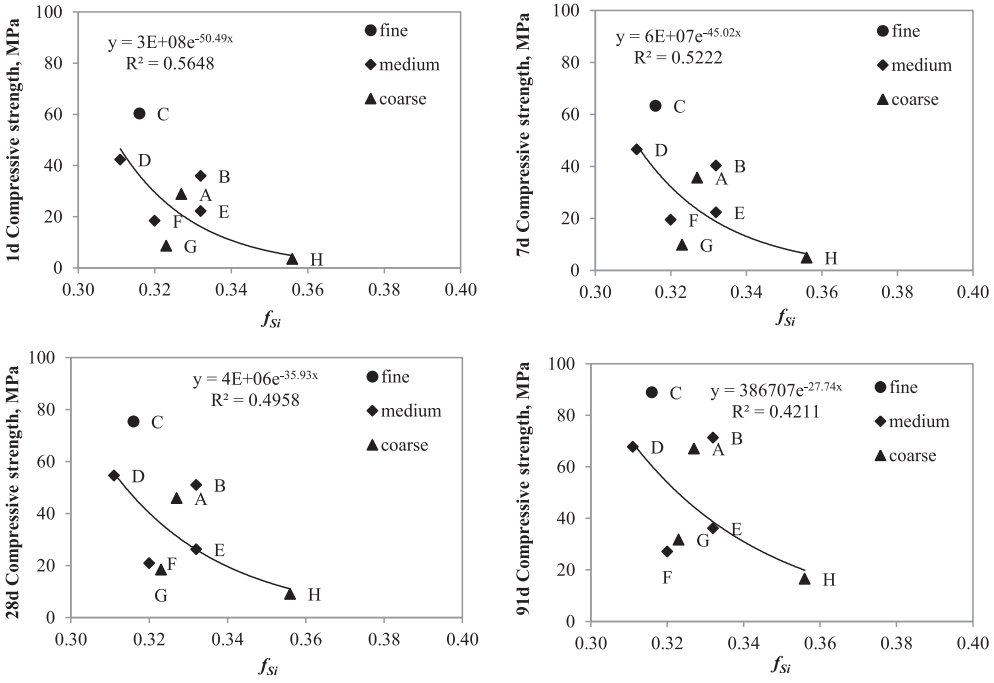

Fig. 10. Effect of degree of polymerization (f_{Si}) on the compressive strength of alkali-activated fly ash pastes.

4. Conclusions

All studied fly ashes can be used to produce alkali-activated materials for the construction industry bearing in mind that fly ashes E, F, G and H are better suited to low strength applications.

There is a strong correlation between Blaine specific surface area of a fly ash, adjusted by the shape factor, and early compressive strength of alkali-activated fly ash paste.

The proposed K-value, which characterizes fly ash reactivity in alkali-activated systems, can be used with a high level of confidence for estimation of strength development of alkali-activated fly ash materials, especially at early age, when calibrated to a specific activator and curing conditions.

The K-value can be effectively used as a comparative instrument for ranking available fly ashes which could be effectively used in industrial-scale production of alkali-activated fly ash materials to monitor quality of the raw material.

The proposed technique (K-value) can be considered as

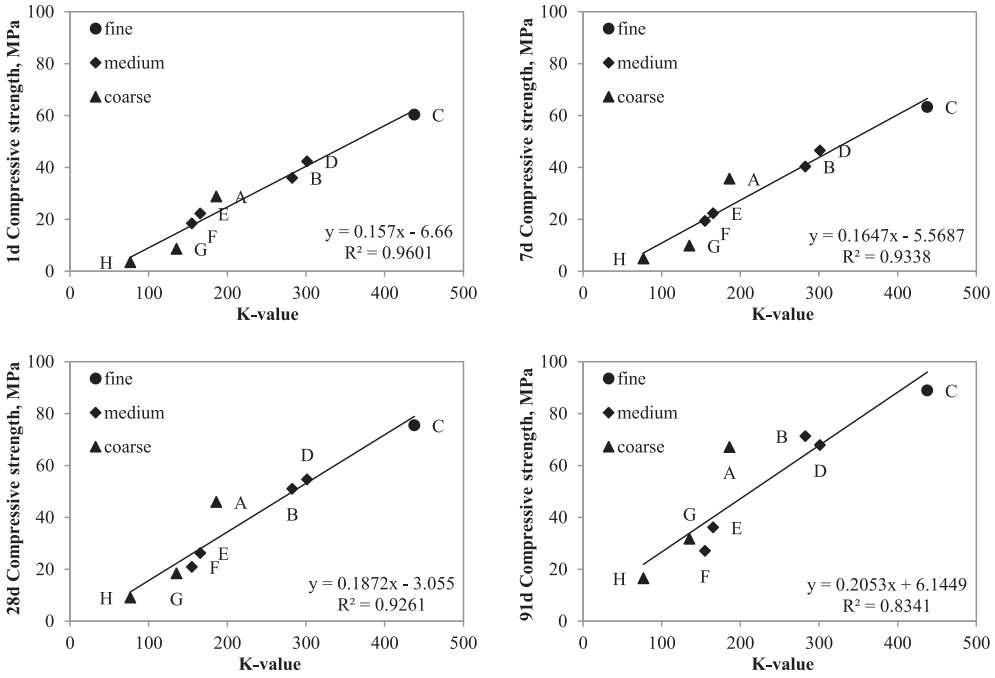

Fig. 11. K-value and compressive strength of alkali-activated fly ash pastes relationship.

sufficiently expressive, since it should be fairly easy to organize routine analyses of particle size distribution, chemical and mineralogical compositions of fly ash and automate (algorithmize) calculations according to Equation (3).

Further refinement and calibration of the proposed reactivity index is needed to provide the construction industry with a powerful robust tool for quality control of fly ashes for alkali-activated materials production, opening new opportunities for large-scale utilization of the waste product.

Acknowledgments

The authors would like to thank: the Department of Research and Innovation of the University of Pretoria for the financial support of Julia Shekhovtsova during her postdoctoral fellowship program; the Ministry of Education and Science of the Russian Federation for sponsoring research of Natalia Kozhukhova and Igor Zhernovsky performed within the framework of this paper (№ 7.872.2017/4.6 Development of principles for the design of ecologically positive composite materials with prolonged bioresistance 2017–2019); Wiebke Grote and Jeanette Strydom for performed XRD and XRF; André Botha from the Laboratory of Microscopy and Microanalysis of the University of Pretoria for providing access to the microscope and assistance during the investigation; Ash Resources and Ulula fly ash for providing fly ashes for the project.

Appendix A

$$SiO_2^{Amorph} = SiO_2^{Total} - \left(C_{Quartz} + SiO_2^{Mullite}\right), \quad (A.1)$$

$$Al_2O_3^{Amorph} = Al_2O_3^{Total} - Al_2O_3^{Mullite}, \quad (A.2)$$

$$Fe_2O_3^{Amorph} = Fe_2O_3^{Total} - \left(Fe_2O_3^{Magnetite} + Fe_2O_3^{Hematite}\right), \quad (A.3)$$

$$CaO^{Amorph} = CaO^{Total} - C_{Lime}, \quad (A.4)$$

$$MgO^{Amorph} = MgO^{Total} - C_{Periclase}. \quad (A.5)$$

where, C - is the mass concentration of a crystalline phase, obtained through XRD analysis (Table 3).

The amorphous SiO_2 and Al_2O_3 contents were calculated using Equations (A.6) And (A.7).

$$SiO_2^{Amorph} = SiO_2^{Total} - \left(C_{Quartz} + \frac{mM_{SiO_2}}{mM_{SiO_2} + nM_{Al_2O_3}} C_{Mullite}\right), \quad (A.6)$$

$$Al_2O_3^{Amorph} = Al_2O_3^{Total} - \frac{nM_{Al_2O_3}}{mM_{SiO_2} + nM_{Al_2O_3}} C_{Mullite}, \quad (A.7)$$

where, n and m – coefficients from brutto-formula of mullite (Table 4).

M_{SiO_2} and $M_{Al_2O_3}$ – molecular masses of SiO_2 and Al_2O_3.

$\frac{mM_{SiO_2}}{mM_{SiO_2}+nM_{Al_2O_3}}$ and $\frac{nM_{Al_2O_3}}{mM_{SiO_2}+nM_{Al_2O_3}}$ mass fractions of SiO_2 and Al_2O_3 in mullite.

For the calculation of the amorphous phase compositions magnetite (Fe_3O_4) will be expressed as molecules of hematite (Fe_2O_3), using the ratio of molecular mass of magnetite to molecular mass of hematite of 1.45. Equation (A.3) will take the form of Equation (A.8):

$$Fe_2O_3^{Amorph} = Fe_2O_3^{Total} - \left(\frac{C_{Magnetite}}{1,45} + C_{Hematite}\right) \quad (A.8)$$

References

Appen, A.A., 1974. Khimia ctekla/Chemistry of glass (in Russian). Khimiya.

ASTM C 1437, 2001. Standard test method for flow of hydraulic cement mortar. ASTM Int.

Bumrongjaroen, W., Muller, I., Schweitzer, J., Livingston, R.A., 2007. Application of glass corrosion tests to the reactivity of fly ash. In: World of Coal Ash (WOCA), Northern Kentuky, USA.

Caglioti, G., Paoletti, A., Ricci, F.P., 1958. Choice of collimators for a crystal spectrometer for neutron diffraction. Nucl. Instrum. 3, 223–228. https://doi.org/10.1016/0369-643X(58)90029-X.

Criado, M., Fernández-Jimenez, A., Palomo, A., Sobrados, I., Sanz, J., 2008. Effect of the SiO2/Na2O ratio on the alkali activation of fly ash. Part II: 29Si MAS-NMR Survey. Microporous Mesoporous Mater. 109, 525–534. https://doi.org/10.1016/j.micromeso.2007.05.062.

Dalby, K.N., King, P.L., 2006. A new approach to determine and quantify structural units in silicate glasses using micro-reflectance Fourier-Transform infrared spectroscopy. Am. Mineral. 91, 1783–1793. https://doi.org/10.2138/am.2006.2075.

De Vargas, A.S., Dal Molin, D.C.C., Vilela, A.C.F., Silva, F.J. Da, Pavão, B., Veit, H., 2011. The effects of Na2O/SiO2 molar ratio, curing temperature and age on compressive strength, morphology and microstructure of alkali-activated fly ash-based geopolymers. Cement Concr. Compos. 33, 653–660. https://doi.org/10.1016/j.cemconcomp.2011.03.006.

Dove, P.M., Han, N., Wallace, A.F., De Yoreo, J.J., 2008. Kinetics of amorphous silica dissolution and the paradox of the silica polymorphs. Proc. Natl. Acad. Sci. U. S. A. 105, 9903–9908. https://doi.org/10.1073/pnas.0803798105.

Dubrovo, S.K., 1958. Reaction of glassy sodium silicates and aluminosilicates with aqueous solutions 8. Action of acid solutions on glassy sodium aluminosilicates with variable acid number. Bull. Acad. Sci. USSR Div. Chem. Sci. 7, 1117–1123. https://doi.org/10.1007/BF00914938.

Duxson, P., 2009. Geopolymer precursor design. In: Provis, J.L., van Deventer, J.S.J. (Eds.), Geopolymers. Structure, Processing, Properties and Industrial Application. Part I. Geopolymer Synthesis and Characterization. Woodhead Publishing Limited, pp. 37–49. https://doi.org/10.1533/9781845696382.1.37.

Duxson, P., Lukey, G.C., van Deventer, J.S.J., 2007. The thermal evolution of metakaolin geopolymers: Part 2 - phase stability and structural development. J. Non-Cryst. Solids 353, 2186–2200. https://doi.org/10.1016/j.jnoncrysol.2007.02.050.

Falk, M., Thomas, R.E., 1974. Molecular size distribution in random polyfunctional condensation with or without ring formation: computer simulation. Can. J. Chem. XXXIII52, 3285–3295. https://doi.org/10.1007/s13398-014-0173-7.2//10.1139/v74-485.

Fernández-Jimenez, A., De La Torre, A.G., Palomo, A., López-Olmo, G., Alonso, M.M., Aranda, M.A.G., 2006. Quantitative determination of phases in the alkali activation of fly ash. Part I. Potential ash reactivity. Fuel 85, 625–634. https://doi.org/10.1016/j.fuel.2005.08.014.

Fernández-Jiménez, A., de la Torre, A.G., Palomo, A., López-Olmo, G., Alonso, M.M., Aranda, M.A.G., 2006a. Quantitative determination of phases in the alkaline activation of fly ash. Part II: degree of reaction. Fuel 85, 1960–1969. https://doi.org/10.1016/j.fuel.2006.04.006.

Fernández-Jiménez, A., Palomo, A., Sobrados, I., Sanz, J., 2006b. The role played by the reactive alumina content in the alkaline activation of fly ashes. Microporous Mesoporous Mater. 91, 111–119. https://doi.org/10.1016/j.micromeso.2005.11.015.

Fernández-Jiménez, A., Palomo, A., 2003. Characterisation of fly ashes. Potential reactivity as alkaline cements. Fuel 82, 2259–2265. https://doi.org/10.1016/S0016-2361(03)00194-7.

Fernández-Jiménez, A., Palomo, J.G., Puertas, F., 1999. Alkali-activated slag mortars: mechanical strength behaviour. Cem. Concr. Res. 29, 1313–1321. https://doi.org/10.1016/S0008-8846(99)00154-4.

Fraser, D.G., 1977. Thermodynamic properties of silicate melts. In: Fraser, D.G. (Ed.), Thermodynamics in Geology: Proceedings of the NATO Advanced Study Institute Held in Oxford, England, September 17–27, 1976. Springer Netherlands, Dordrecht, pp. 301–325. https://doi.org/10.1007/978-94-010-1252-2_15.

Gramenitsky, E.N., Kotelnikov, A.P., Batanova, A.M., Schekina, T.I., Plechyov, P.Y., 2000. Eksperimentalnaya i technicheskaya petrologia/Experimental and technical petrology (in Russian). Naychnii Mir.

Hess, P.C., 1977. Structure of silicate melts. Can. Mineral. 15, 162–177.

Hopkins, C.J., Cabrera, J.G., 1984. The shape factor: a parameter to assess the effect of pulverized fuel ash on the flow properties of cement pastes and concrete. In: International Symposium on Cement and Concrete Science. Beijing, China.

Hunger, M., Brouwers, H.J.H., 2009. Flow analysis of water-powder mixtures: application to specific surface area and shape factor. Cement Concr. Compos. 31, 39–59. https://doi.org/10.1016/j.cemconcomp.2008.09.010.

Kolb, K.E., Hansen, K.W., 1965. Silica structure in borate glasses. J. Am. Ceram. Soc. 48, 439. https://doi.org/10.1111/j.1151-2916.1965.tb14789.x.

Koshukhova, N., Zhernovsky, I., Sobolev, K., 2014. The effect of silica polymerization in fly ash on the strength of geopolymers. MRS Proc. 1611 https://doi.org/10.1557/opl.2014.760 imrc2013-4a-108.

Kovtun, M., Ziolkowski, M., Shekhovtsova, J., Kearsley, E., 2016. Direct electric curing of alkali-activated fly ash concretes: a tool for wider utilization of fly ashes. J. Clean. Prod. 133, 220–227. https://doi.org/10.1016/j.jclepro.2016.05.098.

Kuryaeva, R.G., 2004. Degree of polymerization of aluminosilicate glasses and melts. Glass Phys. Chem. 30, 157–166. https://doi.org/10.1023/B:GPAC.0000024000.19443.f6.

Lacy, E.D., 1965. A statistical model of polymerization/depolymerization relationships in silicate melts and glasses. Phys. Chem. Glasses 6, 171–180.

Lentz, C.W., 1964. Silicate minerals as sources of trimethylsilyl silicates and silicate structure analysis of sodium silicate solutions. Inorg. Chem. 3, 574–579. https://doi.org/10.1021/ic50014a029.

Longhi, M.A., Rodríguez, E.D., Bernal, S.A., Provis, J.L., Kirchheim, A.P., 2016. Valorisation of a kaolin mining waste for the production of geopolymers. J. Clean. Prod. 115, 265–272. https://doi.org/10.1016/j.jclepro.2015.12.011.

Machacek, J., Gedeon, O., Liska, M., 2006. Group connectivity in binary silicate glasses. J. Non-Cryst. Solids 352, 2173–2179. https://doi.org/10.1016/j.jnoncrysol.2006.01.036.

Masson, C.R., 1977. Anionic composition of glass-forming melts. J. Non-Cryst. Solids 25, 1–41.

Masson, C.R., 1968. Ionic equilibria in liquid silicates. J. Am. Ceram. Soc. 51, 134–143. https://doi.org/10.1111/j.1151-2916.1968.tb11856.x.

McLellan, B.C., Williams, R.P., Lay, J., Van Riessen, A., Corder, G.D., 2011. Costs and carbon emissions for geopolymer pastes in comparison to ordinary portland cement. J. Clean. Prod. 19, 1080–1090. https://doi.org/10.1016/j.jclepro.2011.02.010.

Nazari, A., Sanjayan, J.G., 2015. Synthesis of geopolymer from industrial wastes. J. Clean. Prod. 99, 297–304. https://doi.org/10.1016/j.jclepro.2015.03.003.

Nie, Q., Hu, W., Ai, T., Huang, B., Shu, X., He, Q., 2016. Strength properties of geopolymers derived from original and desulfurized red mud cured at ambient temperature. Construct. Build. Mater. 125, 905–911. https://doi.org/10.1016/j.conbuildmat.2016.08.144.

Palomo, A., Grutzeck, M.W., Blanco, M.T., 1999. Alkali-activated fly ashes: a cement for the future. Cem. Concr. Res. 29, 1323–1329. https://doi.org/10.1016/S0008-8846(98)00243-9.

Polyakov, V.B., Ariskin, A.A., Shil'dt, A.V., 2010. Analysis of disproportionation of Q n structons in the simulation of the structure of melts in the Na2O-SiO2 system. Glass Phys. Chem. 36, 579–588. https://doi.org/10.1134/S108765961005007X.

Provis, J.L., Duxson, P., Harrex, R.M., van Deventer, J., 2009. Valorisation of fly ashes by geopolymerisation. Glob. NEST J. 11, 147–154.

Rickard, W.D.A., Williams, R., Temuujin, J., van Riessen, A., 2011. Assessing the suitability of three Australian fly ashes as an aluminosilicate source for geopolymers in high temperature applications. Mater. Sci. Eng. A 528, 3390–3397. https://doi.org/10.1016/j.msea.2011.01.005.

SANS 50196-1, 2006. Methods of Testing Cement. Part 1: Determination of Strength.

Sen, S., Tangeman, J., 2008. Evidence for anomalously large degree of polymerization in Mg2SiO4 glass and melt. Am. Mineral. 93, 946–949. https://doi.org/10.2138/am.2008.2921.

Shekhovtsova, J., Kearsley, E.P., Kovtun, M., 2014. Effect of activator dosage, water-to-binder-solids ratio, temperature and duration of elevated temperature curing on the compressive strength of alkali-activated fly ash cement pastes. J. S. Afr. Inst. Civ. Eng. 56, 44–52.

Shekhovtsova, J., Kovtun, M., Kearsley, E.P., 2016. Temperature rise and initial shrinkage of alkali-activated fly ash cement pastes. Adv. Cem. Res. 28, 3–12. https://doi.org/10.1680/adcr.14.00079.

Shekhovtsova, J., Kovtun, M., Kearsley, E.P., 2015. Evaluation of short-and long- term properties of heat-cured alkali-activated fly ash concrete. Mag. Concr. Res. 67, 897–905. https://doi.org/10.1680/macr.14.00377.

Silva, P. De, Sagoe-Crenstil, K., Sirivivatnanon, V., 2007. Kinetics of geopolymerization: role of Al2O3 and SiO2. Cem. Concr. Res. 37, 512–518. https://doi.org/10.1016/j.cemconres.2007.01.003.

Solovyov, L.A., 2004. Full-profile refinement by derivative difference minimization. J. Appl. Crystallogr. 37, 743–749. https://doi.org/10.1107/S0021889804015638.

Somna, K., Jaturapitakkul, C., Kajitvichyanukul, P., Chindaprasirt, P., 2011. NaOH-activated ground fly ash geopolymer cured at ambient temperature. Fuel 90, 2118–2124. https://doi.org/10.1016/j.fuel.2011.01.018.

Soutsos, M., Boyle, A.P., Vinai, R., Hadjierakleous, A., Barnett, S.J., 2016. Factors influencing the compressive strength of fly ash based geopolymers. Construct. Build. Mater. 110, 355–368. https://doi.org/10.1016/j.conbuildmat.2015.11.045.

Steveson, M., Sagoe-Crentsil, K., 2005. Relationships between composition, structure and strength of inorganic polymers : Part 2 Fly ash-derived inorganic polymers. J. Mater. Sci. 40, 4247–4259. https://doi.org/10.1007/s10853-005-2794-x.

Topçu, İ.B., Toprak, M.U., Uygunoğlu, T., 2014. Durability and microstructure characteristics of alkali activated coal bottom ash geopolymer cement. J. Clean. Prod. 81, 211–217. https://doi.org/10.1016/j.jclepro.2014.06.037.

Jaarsveld, J.G.S. Van, Deventer, J.S.J. Van Van Jaarsveld, J.G.S., Van Deventer, J.S.J., Lorenzen, L., 1997. The potential use of geopolymeric materials to immobilise toxic Metals : Part 1. Theory and applications. Miner. Eng. 10, 1–10. https://doi.org/10.1016/S0892-6875(97)00046-0.

Wang, M.R., Jia, D.C., He, P.G., Zhou, Y., 2011. Microstructural and mechanical characterization of fly ash cenosphere/metakaolin-based geopolymeric composites. Ceram. Int. 37, 1661–1666. https://doi.org/10.1016/j.ceramint.2011.02.010.

Ward, C.R., French, D., 2006. Determination of glass content and estimation of glass composition in fly ash using quantitative X-ray diffractometry. Fuel 85, 2268–2277. https://doi.org/10.1016/j.fuel.2005.12.026.

Williams, R.P., Van Riessen, A., 2010. Determination of the reactive component of fly ashes for geopolymer production using XRF and XRD. Fuel 89, 3683–3692. https://doi.org/10.1016/j.fuel.2010.07.031.

Winnefeld, F., Leemann, A., Lucuk, M., Svoboda, P., Neuroth, M., 2010. Assessment of

phase formation in alkali activated low and high calcium fly ashes in building materials. Construct. Build. Mater. 24, 1086–1093. https://doi.org/10.1016/j.conbuildmat.2009.11.007.

Yang, K.-H., Song, J.-K., Song, K.-I., 2013. Assessment of CO2 reduction of alkali-activated concrete. J. Clean. Prod. 39, 265–272. https://doi.org/10.1016/j.jclepro.2012.08.001.

Zhang, M., El-Korchi, T., Zhang, G., Liang, J., Tao, M., 2014. Synthesis factors affecting mechanical properties, microstructure, and chemical composition of red mud-fly ash based geopolymers. Fuel 134, 315–325. https://doi.org/10.1016/j.fuel.2014.05.058.

Zhang, Z., Provis, J.L., Wang, H., Bullen, F., Reid, A., 2013. Quantitative kinetic and structural analysis of geopolymers. Part 2. Thermodynamics of sodium silicate activation of metakaolin. Thermochim. Acta 565, 163–171. https://doi.org/10.1016/j.tca.2013.01.040.

Zhang, Z., Provis, J.L., Zou, J., Reid, A., Wang, H., 2016. Toward an indexing approach to evaluate fly ashes for geopolymer manufacture. Cem. Concr. Res. 85, 163–173. https://doi.org/10.1016/j.cemconres.2016.04.007.

Zhang, Z., Zhu, Y., Yang, T., Li, L., Zhu, H., Wang, H., 2017. Conversion of local industrial wastes into greener cement through geopolymer technology: a case study of high-magnesium nickel slag. J. Clean. Prod. 141, 463–471. https://doi.org/10.1016/j.jclepro.2016.09.147.

Zhao, F.Q., Ni, W., Wang, H.J., Liu, H.J., 2007. Activated fly ash/slag blended cement. Resour. Conserv. Recycl. 52, 303–313. https://doi.org/10.1016/j.resconrec.2007.04.002.

Zhuang, X.Y., Chen, L., Komarneni, S., Zhou, C.H., Tong, D.S., Yang, H.M., Yu, W.H., Wang, H., 2016. Fly ash-based geopolymer: clean production, properties and applications. J. Clean. Prod. 125, 253–267. https://doi.org/10.1016/j.jclepro.2016.03.019.